

The Journal of Physiology

Cell type-specific relationships between spiking and $[Ca^{2+}]_i$ in neurons of the *Xenopus* tadpole olfactory bulb

Bei-Jung Lin, Tsai-Wen Chen and Detlev Schild

J. Physiol. 2007;582;163-175; originally published online Apr 26, 2007;

DOI: 10.1113/jphysiol.2006.125963

This information is current as of August 8, 2007

This is the final published version of this article; it is available at:

<http://jp.physoc.org/cgi/content/full/582/1/163>

This version of the article may not be posted on a public website for 12 months after publication unless article is open access.

The Journal of Physiology Online is the official journal of The Physiological Society. It has been published continuously since 1878. To subscribe to *The Journal of Physiology Online* go to: <http://jp.physoc.org/subscriptions/>. *The Journal of Physiology Online* articles are free 12 months after publication. No part of this article may be reproduced without the permission of Blackwell Publishing: JournalsRights@oxon.blackwellpublishing.com

Cell type-specific relationships between spiking and $[Ca^{2+}]_i$ in neurons of the *Xenopus* tadpole olfactory bulb

Bei-Jung Lin¹, Tsai-Wen Chen^{1,2} and Detlev Schild^{1,2,3}

¹Institute of Physiology, University of Göttingen, Göttingen Germany

²Bernstein Center for Computational Neuroscience, Göttingen, Germany

³DFG-Research Center for Molecular Physiology of the Brain (CMPB), Göttingen, Germany

Multi-neuronal recordings with Ca^{2+} indicator dyes usually relate $[Ca^{2+}]_i$ to action potentials (APs) assuming a stereotypical dependency between the two. However, $[Ca^{2+}]_i$ affects and is affected by numerous complex mechanisms that differ from cell type to cell type, from cell compartment to cell compartment. Moreover, $[Ca^{2+}]_i$ depends on the specific way a cell is activated. Here we investigate, by combining calcium imaging and on-cell patch clamp recordings, the relationship between APs (spiking) and somatic $[Ca^{2+}]_i$ in mitral and granule cells of the olfactory bulb in *Xenopus laevis* tadpoles. Both cell types exhibit ongoing and odour-modulated $[Ca^{2+}]_i$ dynamics. In mitral cells, the occurrence of APs in both spontaneous and odour-evoked situations correlates tightly to step-like $[Ca^{2+}]_i$ increases. Moreover, odorant-induced suppression of spontaneous firing couples to a decrease in $[Ca^{2+}]_i$. In contrast, granule cells show a substantial number of uncorrelated events such as increases in $[Ca^{2+}]_i$ without APs occurring or APs without any effect upon $[Ca^{2+}]_i$. The correlation between spiking and $[Ca^{2+}]_i$ is low, possibly due to somatic NMDAR-mediated and subthreshold voltage-activated Ca^{2+} entries, and thus does not allow a reliable prediction of APs based on calcium imaging. Taken together, our results demonstrate that the relationship between somatic $[Ca^{2+}]_i$ and APs can be cell type specific. Taking $[Ca^{2+}]_i$ dynamics as an indicator for spiking activity is thus only reliable if the correlation has been established in the system of interest. When $[Ca^{2+}]_i$ and APs are precisely correlated, fast calcium imaging is an extremely valuable tool for determining spatiotemporal patterns of APs in neuronal population.

(Received 1 January 2007; accepted after revision 19 April 2007; first published online 26 April 2007)

Corresponding author D. Schild: Department of Neurophysiology and Cellular Biophysics, Institute of Physiology, University of Göttingen, Humboldtallee 23, 37073 Göttingen, Germany. Email: dschild@gwdg.de

Analysing the signal processing in neuronal networks requires the monitoring of neuronal activities as spatiotemporal patterns. To record from many individual neurons simultaneously, imaging the intracellular calcium concentration ($[Ca^{2+}]_i$) has emerged as one of the most widespread techniques. Because action potentials (APs) cause an influx of Ca^{2+} through voltage-activated Ca^{2+} channels, $[Ca^{2+}]_i$ is often assumed to parallel neuronal electrical activity. Accordingly, many laboratories have used somatic $[Ca^{2+}]_i$ as an indicator for electrical activity assuming a high correlation between the two (Czesnik *et al.* 2003; Ohki *et al.* 2005; Sullivan *et al.* 2005).

However, $[Ca^{2+}]_i$ can also be affected by processes not driven by APs such as subthreshold activation of low-voltage-activated Ca^{2+} channels (Perez-Reyes,

2003), activation of Ca^{2+} -permeable receptors (Kovalchuk *et al.* 2000) or Ca^{2+} release from intracellular calcium stores (Kuba *et al.* 1992; Zufall *et al.* 2000). Moreover, elevated $[Ca^{2+}]_i$ may activate Ca^{2+} -dependent potassium or chloride conductances and thereby reduce a cell's excitability and inhibit spiking (Sah, 1996). Thus, the degree of correlation between $[Ca^{2+}]_i$ and APs may depend on the $[Ca^{2+}]_i$ handling machinery in a specific compartment of a specific cell type and on the way cells are activated.

Here we show that the relationships between somatic $[Ca^{2+}]_i$ and electrical activity can differ markedly among the cell types of the same brain area, taking mitral cells (MCs) and granule cells (GCs) of the olfactory bulb (OB) of *Xenopus laevis* tadpoles as an example. Our results highlight the importance of characterizing the relationship in every particular cell type under investigation.

This paper has online supplemental material.

Methods

Olfactory slice preparation

Tadpoles of *Xenopus laevis* (stage 50–54; Nieuwkoop & Faber, 1956) were immobilized by cooling in iced water for approximately 5 min, followed by transection of the brain at the level of the midbrain. A block of tissue containing the olfactory mucosae, the olfactory nerves and the rostral part of the brain was isolated and kept in frog Ringer solution containing (mM): 98 NaCl, 2 KCl, 1 MgCl₂, 5 glucose, 5 sodium pyruvate, 10 Hepes (230 mosmol l⁻¹, pH 7.8; Sigma). The dorsal part of the OB was sliced off horizontally using a vibrating microtome (Leica VT1000S). Thus, the olfactory mucosae, nerves and all parts of the brain relevant for our experiments were preserved in the preparation. The animal experiment was approved by the Göttingen University Committee for Ethics in Animal Experimentation.

Calcium imaging

For loading the fluorescence indicator, the preparation was incubated in 200 μ l of frog Ringer solution containing 50 μ M fura-2/AM (Molecular Probes) for 30 min. Then it was placed on the stage of a microscope and continuously superfused with Ringer solution for 30 min to remove dye in the extracellular space and to allow full de-esterification of the dye in the cytoplasm. For fura-2 imaging, excitation bands around 380 nm and 350 nm were selected from a xenon lamp (Zeiss XBO, 75 W) using a custom-built monochromator. An optical fibre coupled the excitation light into an upright microscope (Axioskop 2, Zeiss) equipped with a fura-2 filter set (emission: BP 500–530, dichroic: FT 425, Zeiss). Fluorescence images were recorded using a frame-transfer, back-illuminated CCD camera (Princeton Instruments, MicroMAX: 512BFT) and stored on a PC using Winview32 software (Visitron System, Munich). To prevent bleaching, most imaging experiments were made using only one excitation wavelength (380 nm). For quantitative fluorescence measurements, pairs of images were acquired at excitation wavelengths of 350 and 380 nm.

Under epifluorescence illumination, two cell layers in stained OBs could be easily distinguished (Fig. 1). According to a previous study in the same preparation (Czesnik *et al.* 2001), cells in the rostral layer project their axons out of the bulb and their dendrites into glomeruli where their terminals form tufts, a characteristic branching structure of mitral/tufted cells (Fig. 1C). In the caudal layer, most cells are axonless interneurons bearing numerous spines on their dendrites (Fig. 1D). In this study, we identified cell types based on their soma location in a specific layer, namely cells in the rostral cell layer as mitral cells (MCs) and cells in the caudal layer as granule cells (GCs). It has, however, to be borne in mind that

MCs migrate through the granule cell layer before they reach their final position in the mitral cell layer (Hinds, 1968*a,b*). Some immature, migrating MCs have therefore to be expected in the granule cell layer.

Odorant stimulation and stimulus responses

A mixture of 14 L-amino acids (alanine, serine, threonine, cysteine, valine, leucine, isoleucine, methionine, proline, arginine, lysine, histidine, phenylalanine and tryptophan, each 200 μ M in frog Ringer solution, Sigma) was used as odorant stimulation to the olfactory receptor neurons. As receptor neurons might respond to pressure changes of the stimulus flow (Zippel & Breipohl, 1975), an odorant application device was used to keep the pressure change lower than 11 mPa while odorant solution was added through the device to the olfactory epithelium (Schild, 1985). As a control, we applied bath solution in the same way as we applied the amino acid mixture to make sure that the responses were due to the amino acids rather than to any other sources.

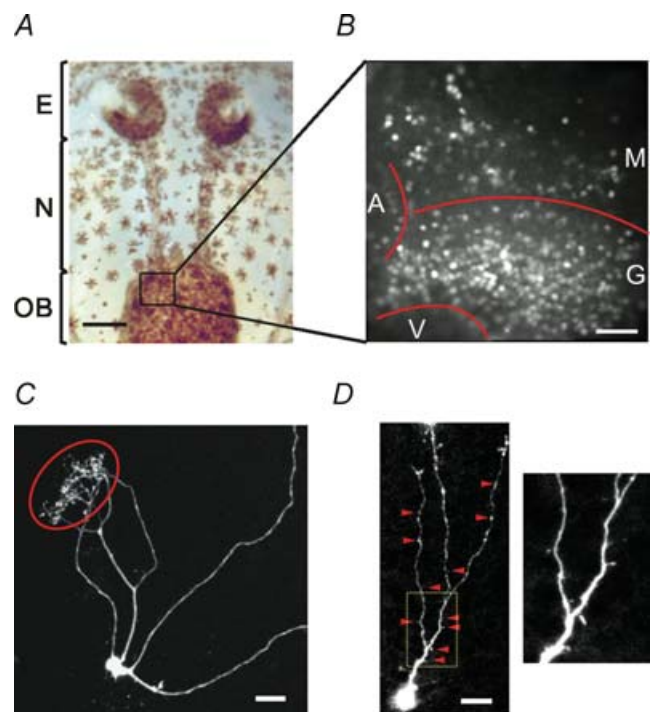


Figure 1. Nose–brain preparation of *Xenopus laevis*

A, the preparation contains the olfactory epithelia, the olfactory nerves, and the olfactory bulbs. E, olfactory epithelium; N, olfactory nerve; OB, olfactory bulb. Scale bar, 1 mm. B, a fluorescence image of the fura-2/AM-loaded olfactory bulb taken at 380 nm excitation. M, mitral cell layer; G, granule cell layer; A, accessory olfactory bulb; V, ventricle. Scale bar, 50 μ m. C, morphology of a cell located in the mitral cell layer. Glomerular tuft encircled. D, morphology of a typical cell in the granule cell layer. Note the dendritic spines (arrowheads; also see inset) along the dendrites. Cells (in C and D) were injected with Alex 488 through a patch pipette and imaged using a confocal microscope. Scale bars in C and D, 20 μ m.

Due to ongoing activity in the OB, some peaks of the spontaneous $[Ca^{2+}]_i$ fluctuations could easily be mistaken for stimulus-induced responses. We therefore recorded ongoing $[Ca^{2+}]_i$ activity for 1 min, and then applied three identical stimuli, one each minute. A response was assumed if the correlation coefficients between trials had an average value above 0.4. The three response waveforms were then averaged to extract a stimulus-specific component.

Combined calcium imaging and on-cell patch clamp recordings

For simultaneous measurements of $[Ca^{2+}]_i$ and APs, we combined fura-2 imaging with on-cell, loose-seal patch-clamp recording. Neurons were first loaded with fura-2/AM and a full size $[Ca^{2+}]_i$ image sequence was taken to record $[Ca^{2+}]_i$ signals of many neurons. Image sequences were then analysed immediately and a cell showing either spontaneous $[Ca^{2+}]_i$ fluctuations or odour-evoked $[Ca^{2+}]_i$ responses was selected and reidentified in transmission optics. After the on-cell patch clamp configuration was established on the selected cell, simultaneous patch-clamp and $[Ca^{2+}]_i$ recordings were carried out. Patch pipettes were pulled from borosilicate micropipettes (o.d. 1.8 mm; Hilgenberg, Germany). Pipette resistances were 2–3 M Ω when filled with a solution containing (mM): 98 NaCl, 2 KCl, 3 MgCl₂, 10 Hepes, and 0.2 EGTA (pH 7.8). A small positive pressure (~30 hPa) was constantly applied to the pipette while approaching the cell. When a pipette tip was placed against a cell membrane, the release of positive pressure was sufficient for the seal resistance to increase to 20–50 M Ω . Capacitive currents induced by APs were recorded using an EPC-7 patch-clamp amplifier in the voltage clamp mode at 0 mV holding voltage. The signal was then filtered with the built-in Bessel filter at 3 kHz, digitized at 10 kHz, and stored to disk using a custom-built hardware and software. Image acquisition was triggered by the patch-clamp software for synchronizing patch recordings with CCD image acquisition. The trigger times were written to the patch-clamp data file to allow off-line data alignment. For fast CCD imaging, $[Ca^{2+}]_i$ was sampled at 125 Hz by binning all pixels of a recorded cell.

The loose-seal configuration was used because, under tight seal conditions (> 1 G Ω), we had observed $[Ca^{2+}]_i$ increases after the glass pipette touched the cell membrane (a similar effect was described in rat somatotropes; Robert *et al.* 1999). A low seal resistance of 20–50 M Ω in the on-cell configuration allowed spike detection while preserving a normal $[Ca^{2+}]_i$ activity. We further recorded $[Ca^{2+}]_i$ responses of the cell of interest prior to and after the loose patch was established to confirm that patch recordings did not alter the $[Ca^{2+}]_i$ activity.

Simultaneous whole-cell patch clamp recordings and calcium imaging

To clamp the membrane potential in the subthreshold voltage range, we performed whole-cell patch clamp experiments. Patch pipettes with pipette resistance of 6–8 M Ω were loaded with the following solution (mM): 2 NaCl, 1 KCl, 2 MgSO₄, 90 potassium gluconate, 10 Hepes, 3 K-ATP, 0.3 K-GTP and 0.05 K-fura-2. Preparations were continuously perfused with Ringer solution throughout the experiments. After the whole-cell configuration was established, the membrane potential was held at –85 mV and then clamped for 800 ms at various voltages ranging from –75 to –25 mV. Meanwhile, calcium imaging was done simultaneously in the voltage-clamped cell.

NMDA puff application

A sequence of calcium images was taken from a region of the OB while a focal NMDA puff was applied to one of the imaged somata. A fast perfusion system was placed near the puffer pipette to create a constant, anterior-to-posterior flux of bath solution, which quickly diluted the NMDA applied and removed it from the extracellular space, thereby preventing the activation of dendritic NMDARs of the imaged cell. The bath solution contained (mM): 98 NaCl, 2 KCl, 1 MgCl₂, 0.01 glycine, 5 glucose, 5 sodium pyruvate, 10 Hepes and 5 μ M TTX to block Na⁺-dependent APs. Patch pipettes with resistance of 6 M Ω were loaded with bath solution containing 100 μ M NMDA. Short pressure pulses (3.4 kPa; 1 s) were delivered by a pneumatic ejection system (PDES-2L npi Electronics, Germany) and were used to eject a small amount of NMDA solution. As a control we added a fluorophore to the puffer pipette to monitor the flow of ejected solution and confirmed that the ejected solution spread only locally, close to the cell body of the target cell (see online Supplemental material, Movie 1).

Data analysis

Imaging analysis was done using Matlab (MathWorks). For quantitative image analysis, two fluorescence intensities measured from two excitation wavelengths were used, and the ratios of the background-subtracted fluorescence values (Chen *et al.* 2006) at the two wavelengths were calculated to cancel effects of optical path length and dye amount. Otherwise, the fluorescence intensity time course $F(t)$ was calculated by averaging the pixels corresponding to the soma. Because the emission of fura-2 when excited at 380 nm decreases with increasing $[Ca^{2+}]_i$, we represented the fluorescence traces as the normalized relative fluorescence $F_n(t) = (F_{\max} - F(t))/F_{\max}$, F_{\max} being the maximum of $F(t)$.

For ratio measurements, the background-corrected fluorescence values at excitation 350 nm and 380 nm were

taken to calculate their ratio, $r = F_{350}/F_{380}$, which gives a time function $r(t_i)$ of ratios with t_i being the time of image acquisition. To indicate changes of $[Ca^{2+}]_i$, i.e. $\Delta[Ca^{2+}]_i$, we took the changes in ratios, i.e. $\Delta r(t_i) = r(t_i) - r(t_{i-1})$.

To quantify the level of spontaneous $[Ca^{2+}]_i$ fluctuations, we proceeded as follows. First, we distinguished a significant increase in fluorescence from an increase caused by noise by applying the paired t test to the intensities of a cell's individual pixels at t and at $t + dt$. The time point t was included as part of a rising phase if the test was significant at a level $P < 0.001$. Second, we calculated the proportion of significant rising phases to the total time of the trace, and named this proportion the 'mean activity index' (MAI; Fig. 2B).

In order to determine the points in time where AP-related currents occurred in the recorded current traces, the cross-correlation function between an AP-associated current template and the whole current trace was calculated. Peaks of this function indicated the occurrences of APs. The timing and the amplitudes of AP-related currents were then obtained from the current traces and were used for quantifying the strength of correlation between APs and $[Ca^{2+}]_i$ fluctuations. Data are presented as means \pm s.e.m. Significance was determined using the Mann–Whitney U test.

Results

We investigated spontaneous and odorant-induced spiking and $[Ca^{2+}]_i$ activities in a nose–brain preparation (Fig. 1A). This preparation allows the imaging of a large ensemble of neurons in the CNS while stimulating the olfactory epithelium with odors. Fluorescence images of the main OB were taken using fura-2/AM-loaded preparations. Two cell layers (Fig. 1B) could be identified corresponding to the mitral and the granule cell layer (Nezlin & Schild, 2000; Czesnik *et al.* 2001). We then systematically investigated the spontaneous and odorant-evoked $[Ca^{2+}]_i$ activity in MCs and GCs and analysed how the $[Ca^{2+}]_i$ dynamics was related to spiking activity.

Ongoing $[Ca^{2+}]_i$ fluctuations

Time series of $[Ca^{2+}]_i$ images were recorded from MCs and GCs (390 cells in 10 slices; 186 MCs and 204 GCs) without odorant stimulation. In both cell types, we observed prominent ongoing $[Ca^{2+}]_i$ fluctuations. Amplitudes and frequencies of the fluctuations varied from cell to cell as exemplified by the traces shown in Fig. 2A.

To quantify the spontaneous $[Ca^{2+}]_i$ fluctuations, we summed the durations of individual rising phases (Fig. 2B; marked in red), expressed it as the percentage

of the recording period and called it the 'mean activity index' (MAI) (see Methods). On the average, MCs had a higher MAI than GCs (0.219 ± 0.009 for MCs, $n = 186$; 0.053 ± 0.003 for GCs, $n = 204$, $P < 0.005$; Fig. 2C). According to the cumulative probability plot, approximately 90% of MCs showed substantial $[Ca^{2+}]_i$ fluctuations (MAI > 0.05), while only 46% of GCs displayed the same level of fluctuations (Fig. 2D). In addition, highly active cells (MAI > 0.26) were located exclusively in the mitral cell layer resulting in a broader distribution of $[Ca^{2+}]_i$ activity levels in MCs than in GCs (Fig. 2D). Both MCs and GCs showed ongoing $[Ca^{2+}]_i$ activity, but the MC population displayed a higher and broader activity distribution than the GC population.

Relationship between spontaneous $[Ca^{2+}]_i$ fluctuations and APs

To investigate the relationship between somatic $[Ca^{2+}]_i$ and spiking activity, we recorded both activities simultaneously using calcium imaging and on-cell loose patch recording. We placed vertical lines in the fluorescence trace at the times of APs from the on-cell recording (Fig. 3A and B, see Methods). In MCs, the occurrence of APs mostly coincided with $[Ca^{2+}]_i$ increases (Fig. 3B, $n = 12$). To quantify the relationship between $[Ca^{2+}]_i$ increases and the number of APs, we first calculated the ratio, r , of the fluorescence intensities taken at 350 and 380 nm excitation (Fig. 3C, upper panel, along with APs). Time functions of ratio differences, i.e. $\Delta r(t_i) = r(t_i) - r(t_{i-1})$, were then calculated to indicate the changes in $[Ca^{2+}]_i$, and shown in a sliding window of 400 ms (Fig. 3C, middle panel). APs were counted within the same time intervals (Fig. 3C, lower panel). There was an obvious correlation between $\Delta r(t)$ and spike counts, which was also evident when Δr was plotted as a function of the corresponding spike numbers (Fig. 3D). A high $[Ca^{2+}]_i(t)$ –spiking correlation was observed in all cells sampled in the mitral cell layer whereby Δr per spike varied from cell to cell (Fig. 3E). Note that, at this time resolution, one or two spikes per image pair acquisition time did usually not prevent $[Ca^{2+}]_i$ from slowly decaying. This resulted in negative Δr values at low spiking activity (Fig. 3D and E).

When the same measurement as described above for MCs was carried out on GCs, the results were markedly different. In the majority of the GCs sampled, increases in $[Ca^{2+}]_i$ did not appear to be strictly related to the occurrence of APs. We observed numerous APs without any detectable $[Ca^{2+}]_i$ increases associated with them (Fig. 4A).

To quantitatively compare the degree of $[Ca^{2+}]_i(t)$ –spiking correlation in MCs and GCs, we calculated the correlation coefficients (ρ) between $[Ca^{2+}]_i$ increases and the occurrence of spikes. Figure 4A gives

example traces with the corresponding ρ values from MCs and GCs. Traces with larger values of ρ show a high correlation between $[Ca^{2+}]_i$ increases and APs, while traces with smaller values of ρ were characterized by a large number of uncorrelated events. All recorded MCs showed a high correlation ($\rho > 0.5$) between $[Ca^{2+}]_i$ increases and APs, whereas this correlation was significantly lower in GCs ($\rho = 0.37 \pm 0.05$ for GCs, $n = 15$; $\rho = 0.68 \pm 0.03$ for MCs, $n = 12$, $P < 0.005$; Fig. 4B).

Odour-induced modulation of $[Ca^{2+}]_i$ dynamics

As a next step of our analysis, we investigated odour-evoked responses in OB cells. Short pulses of odorants were applied to the olfactory epithelium while sequences of images were taken from the OB (see Methods). Though responses to repeated stimuli varied to a certain extent, they shared a common temporal pattern (Fig. 5A). For

evaluation, regions of interest were chosen in a way that their fluorescence intensities were largely uncorrelated with their neighbourhood (Fig. 5B and C).

In MCs (10 slices, 226 cells), odour stimulation could modulate the spontaneous $[Ca^{2+}]_i$ activity in three different ways (Fig. 5A). Odour could elicit either an increase of $[Ca^{2+}]_i$ (Fig. 5Ad, f and g) or a decreased in $[Ca^{2+}]_i$ (Fig. 5Aa and b) with various durations. In the latter cases the cells usually displayed substantial spontaneous $[Ca^{2+}]_i$ fluctuations so that the response appeared as a suppression of the spontaneous activity. In addition, some MCs showed more complex response consisting of an initial $[Ca^{2+}]_i$ increase followed by a suppression (Fig. 5Ac, e and h). The duration of the suppression varied from several seconds (Fig. 5Ac and e) to minutes (Fig. 5Ah).

Using the same experimental protocol, we also analysed odour-evoked $[Ca^{2+}]_i$ responses in GCs (14 slices, 246

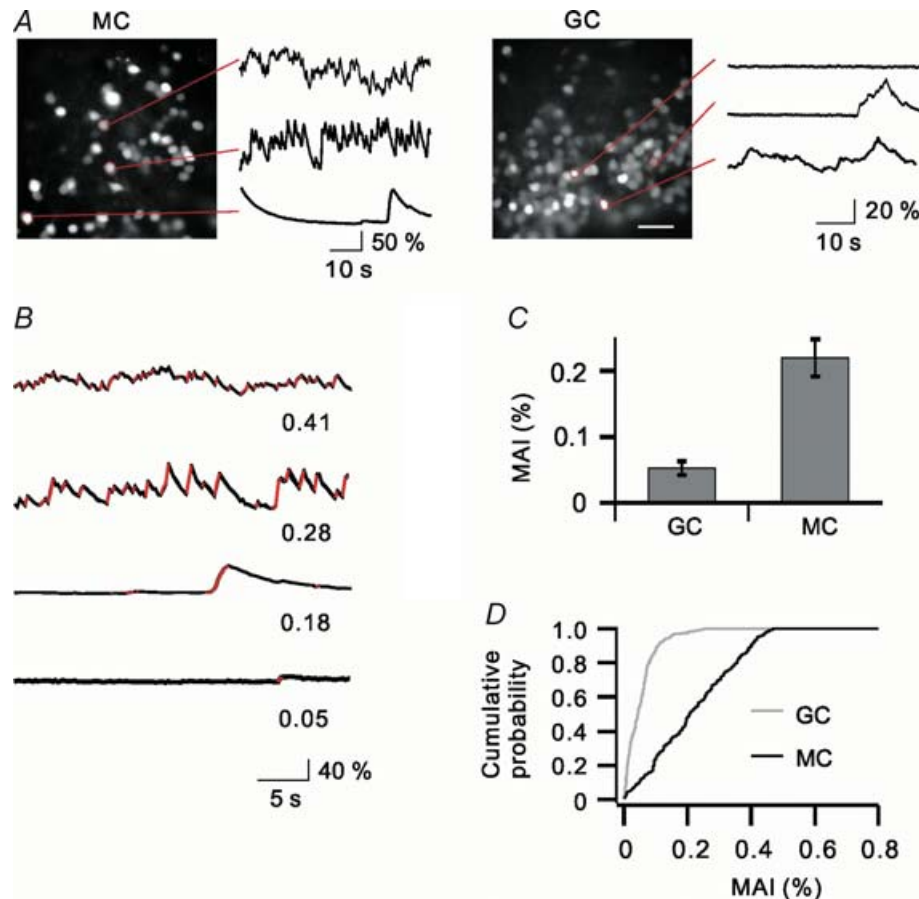


Figure 2. Ongoing $[Ca^{2+}]_i$ fluctuations in bulbar cells

A, in the absence of stimulation, both MCs and GCs show prominent fluctuations of $[Ca^{2+}]_i$ with various amplitudes and frequencies. Example traces from cells encircled in red. Scale bar for both fluorescence images, $30 \mu\text{m}$. B, traces with various degrees of fluctuations. Non-random rising phases are drawn in red. Their overall duration divided by the trace length gives the mean activity index (MAI) as indicated at each trace. C, the MAIs of MCs are significantly higher than those of GCs. D, cumulative frequencies of MAIs in MCs and GCs, with MAI ranging from 0 to 0.5 for MCs and 0–0.26 for GCs.

cells). GCs also produced response waveforms consisting of single or compound $[Ca^{2+}]_i$ transients with different durations (Fig. 5A*i-n*), but suppressive responses in GCs were less frequent.

To summarize the responses in the image data, we represent the normalized relative fluorescence traces, $F_n(t)$, of each cell as a horizontal coloured bar using a colour spectrum from blue (low $[Ca^{2+}]_i$) to red (high $[Ca^{2+}]_i$) (Fig. 5D). In this representation, the response types as well as the response durations are clearly seen. Suppressive $[Ca^{2+}]_i$ responses (lower parts of panels) occurred more frequently in MCs (56%) than in GCs (15%).

Odour-evoked $[Ca^{2+}]_i$ and spiking activity in MCs and GCs

Given the $[Ca^{2+}]_i$ response patterns described above, it was intriguing to investigate how these patterns were related to the electrical odorant responses. To answer this question, we first imaged a population of neurons and then targeted

a responding cell for simultaneous on-cell patch clamp and calcium imaging.

These simultaneous recordings showed a high correlation between $[Ca^{2+}]_i$ responses and odour-evoked spiking patterns in MCs. Whenever odorant stimulation elicited a $[Ca^{2+}]_i$ increase, there were APs coinciding with the rising phase of the $[Ca^{2+}]_i$ signal (Fig. 6A upper trace). On the other hand, when stimulation led to a decrease in $[Ca^{2+}]_i$, this was associated with a suppression of firing (Fig. 6A lower trace). A similar relationship was observed in eight other cells (together with the two above mentioned cells, 5 excitatory and 5 inhibitory; Fig. 6B). Thus in MCs, $[Ca^{2+}]_i$ could reflect both increasing and decreasing spiking rates during sensory stimulation. Taken together, $[Ca^{2+}]_i$ and spiking activity in MCs appeared to be highly correlated during both spontaneous and odour-evoked activity.

When $[Ca^{2+}]_i$ was sampled at the relatively low image acquisition rate, the rising phase of $[Ca^{2+}]_i$ responses appeared to be rather smooth. In order to understand whether this was due to a high calcium buffering

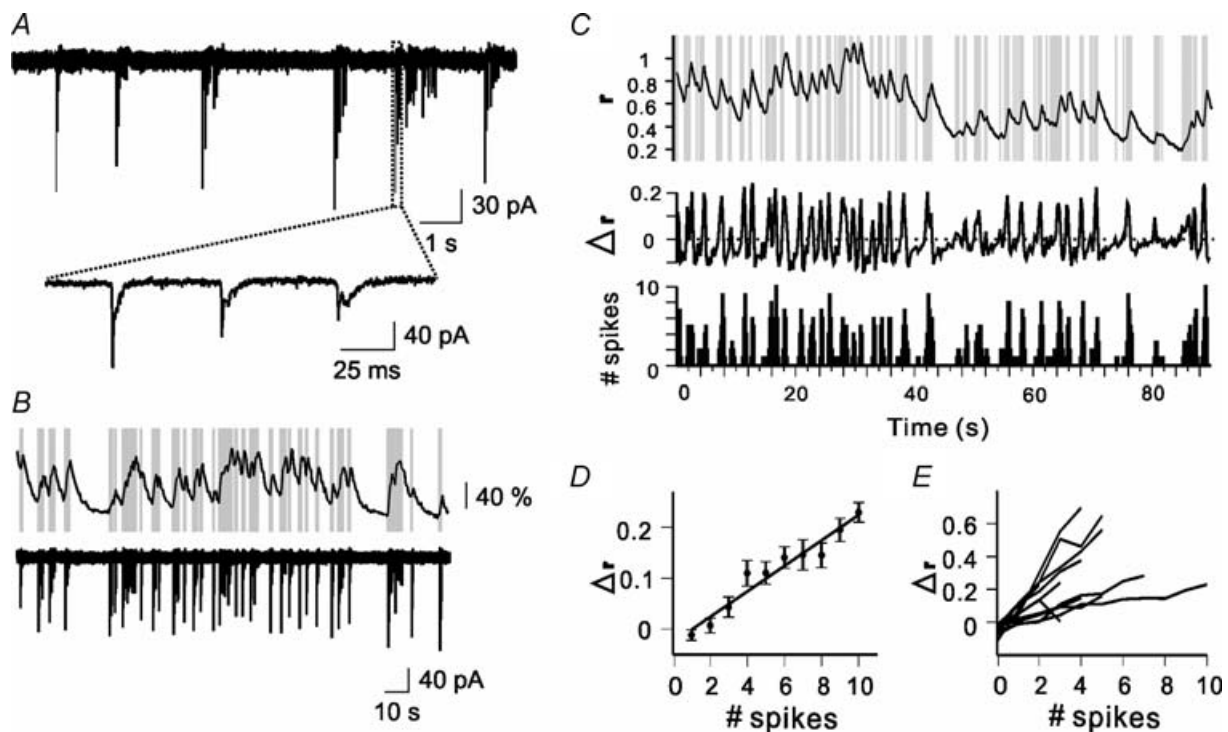


Figure 3. Correlated spiking and $[Ca^{2+}]_i$ activity in MCs

A, on-cell, loose-seal patch-clamp recordings of capacitive currents induced by bursts of APs. Zoomed trace shows typical decay of current amplitudes within a burst. **B**, simultaneous calcium imaging (upper trace) and on-cell recording (lower trace) reveal the correlation between APs and rising phases of the $[Ca^{2+}]_i$ signal in MCs. APs detected in the lower trace are indicated by vertical grey lines in the upper trace. **C**, ratio trace with superimposed APs (upper), differential ratio, Δr (middle), and spike count histogram (lower) of a combined electrophysiological and imaging record. Peaks in the Δr function match the peaks of the spike count histogram. **D**, linear correlation of the Δr and spike counts as shown in **C**. In this case, the correlation coefficient ρ between Δr and spike counts was 0.83. Error bars, mean \pm 3 s.e.m. Least square regression line fit. **E**, same evaluation and regression lines for 12 MCs.

capacity or, alternatively, to the low frame acquisition rate, we performed experiments at a faster imaging rate (667 Hz) using the line scanning mode of a confocal microscope (LSM510). At this rate, we were able to resolve tiny discrete stepwise increments within the overall increase of the $[Ca^{2+}]_i$ response (Fig. 6C). By simultaneous on-cell recordings and fast CCD imaging (a single pixel; 125 Hz), we observed a precise correlation between $[Ca^{2+}]_i$ steps and individual APs (Fig. 6D). Each AP within an odour-evoked burst corresponded to a $[Ca^{2+}]_i$ step. Thus, in MCs, fast $[Ca^{2+}]_i$ imaging can resolve distinct $[Ca^{2+}]_i$ steps corresponding to individual APs.

Unlike the coincidence of $[Ca^{2+}]_i$ increases and APs in MCs, the majority of GCs (11 out of 16 cells) showed uncorrelated events following odour stimulation, i.e. a number of APs failed to elicit any $[Ca^{2+}]_i$ increases (asterisked in Fig. 7A), or $[Ca^{2+}]_i$ increased in the absence of APs (Fig. 7A). Although GCs showed odour-evoked increases of $[Ca^{2+}]_i$ along with an increase in spiking, the latencies or the durations of $[Ca^{2+}]_i$ increases did not match the temporal spiking pattern.

To further examine the relationship between single APs and the temporal fine structure in GC $[Ca^{2+}]_i$ responses, we again combined on-cell recordings with fast calcium imaging. In seven out of the 10 cells recorded, we observed a high number of uncorrelated events. In these cells, $[Ca^{2+}]_i$ either increased before the occurrence of an AP (Fig. 7Ba), or it kept increasing even after the neuron stopped firing (Fig. 7Bb and c). Three cells showed steplike $[Ca^{2+}]_i$ increases upon odorant stimulation, each step corresponding to an individual AP (Fig. 7Bd). In these neurons, spontaneous APs often failed to elicit any $[Ca^{2+}]_i$ increase (Fig. 7Bd, see legend), a behaviour never observed in MCs.

AP-independent $[Ca^{2+}]_i$ increases in GCs

The low correlation between APs and $[Ca^{2+}]_i$ in GCs suggested that the somatic $[Ca^{2+}]_i$ was partly affected by factors not related to APs. For example, the activation of somatic ligand-gated Ca^{2+} -permeable receptors could contribute to $[Ca^{2+}]_i$ influx independent of spiking activity. Specifically, we tested whether NMDA receptors can mediate AP-independent $[Ca^{2+}]_i$ change in MC and GC somata. A brief puff of NMDA was focally applied onto individual somata while their $[Ca^{2+}]_i$ was recorded in the presence of TTX. A fast flux of bath solution (Fig. 8A) kept the stimulus short and prevented the diffusion of NMDA to the rostrally extending dendrites. Focal puffs of NMDA onto GC somata reliably induced $[Ca^{2+}]_i$ increases in 12 out of 16 GC (Fig. 8B). In sharp contrast, when the same experimental procedure was repeated on MC somata, none of the cells tested showed significant change in $[Ca^{2+}]_i$ ($n = 6$; Fig. 8B and C). Thus, if the NMDA receptor on

GC somata are activated during network activity, e.g. by the diffusion of glutamate released from nearby synapses (Shepherd & Greer, 1998; Isaacson & Murphy, 2001), the resulting AP-independent $[Ca^{2+}]_i$ increases could lower the correlation between spiking and $[Ca^{2+}]_i$ in GCs.

In addition to receptor-mediated Ca^{2+} influxes, GCs are known to exhibit a wealth of subthreshold signalling events (Cang & Isaacson, 2003; Pinato & Midtgaard, 2003; Egger *et al.* 2003; Zelles *et al.* 2006) that may also contribute to AP-independent Ca^{2+} influx, e.g. by opening LVA Ca^{2+} channels (Egger *et al.* 2003; Pinato & Midtgaard, 2003). To test this possibility, we clamped GC somata at -85 mV and monitored their $[Ca^{2+}]_i$ dynamics in response to depolarizing steps in the subthreshold voltage range. Prominent $[Ca^{2+}]_i$ increases were observed at GC somata in response to depolarization pulses in the range between -75 and -55 mV ($n = 5$; Fig. 9A and B). Thus, subthreshold membrane potential dynamics can substantially contribute to Ca^{2+} influxes in GCs. Whether subthreshold membrane potential depolarization could

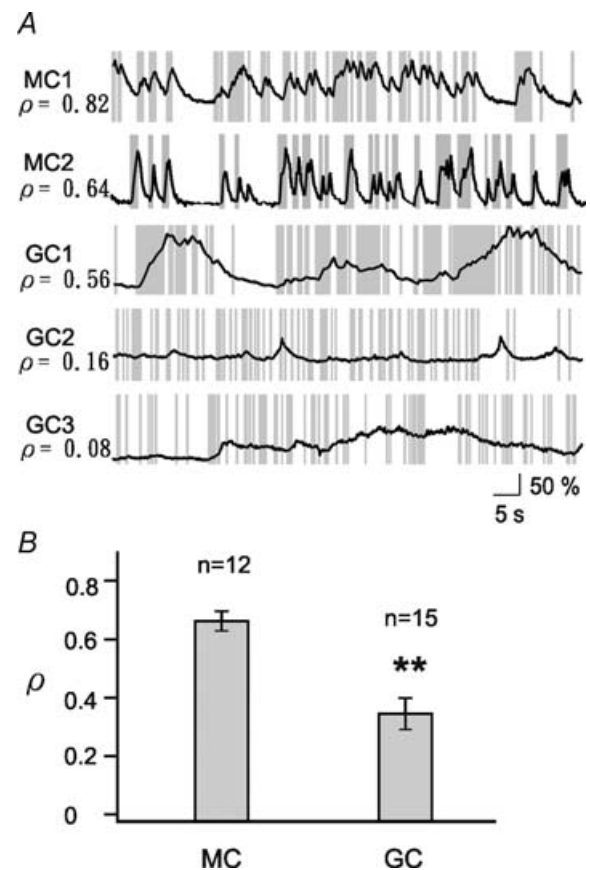


Figure 4. Comparison between MCs and GCs regarding the correlations between spikes and $[Ca^{2+}]_i$ dynamics

A, examples of simultaneous electrical and $[Ca^{2+}]_i$ recordings in MCs (MC1 and MC2) and GCs (GC1, GC2, and GC3). Correlation coefficients (ρ) between Δr and spikes are indicated at each record. B, correlation coefficients for MCs and GCs. There is significantly lower correlation in GCs.

occur during odorant stimulation was further tested using the current-clamp mode of the patch clamp technique. In GCs, odorant stimulation induced a few (standard) APs and numerous subthreshold dendritic spikes (Pinato & Midtgaard, 2005; Zelles *et al.* 2006) superimposed on a long-lasting depolarization (Fig. 9C). Taken together, the AP-independent $[Ca^{2+}]_i$ signal in GCs is likely in

part driven by prominent subthreshold depolarization, in particular during odorant responses.

Discussion

In this study we demonstrated different relationships between somatic $[Ca^{2+}]_i$ dynamics and the occurrence

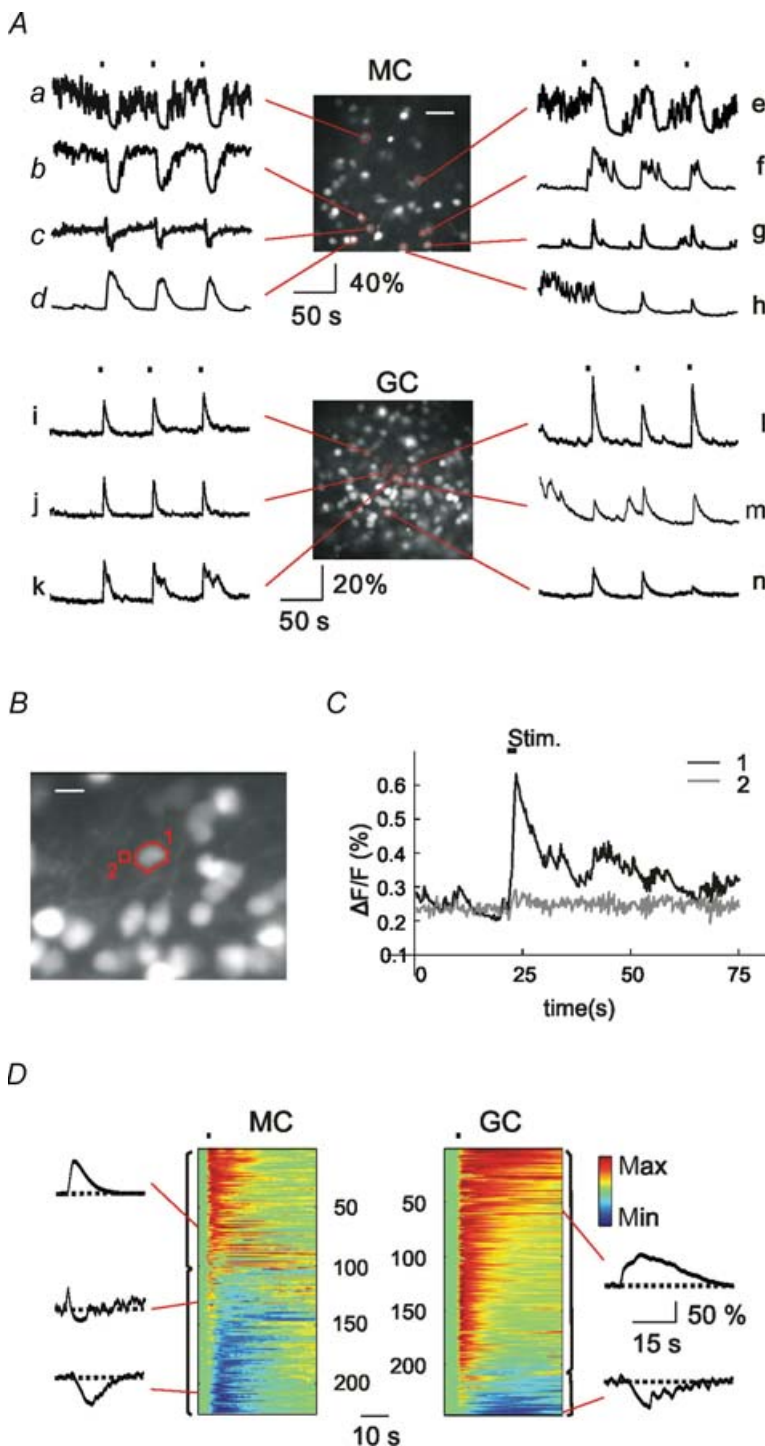


Figure 5. Odour-induced somatic $[Ca^{2+}]_i$ dynamics in MCs and GCs

A, MCs show odour-evoked increases in $[Ca^{2+}]_i$ (*d, f, g*), decreases (*a, b*), or a combination of both (*c, e, h*). GCs respond mostly with an increase in $[Ca^{2+}]_i$ (*i–n*). Filled squares over the traces *a, e, i* and *l* indicate, for all traces, the times of odorant stimulation. Scale bar, for both fluorescence images, $30\ \mu\text{m}$. *B*, fluorescence image of GCs. Two ROIs indicate a soma (1) and a small region (2) close to the soma. Scale bar: $15\ \mu\text{m}$. *C*, two simultaneous fluorescence time traces. The black and grey traces represent the fluorescence signals averaged over pixels in ROI (1) and ROI (2), respectively. *D*, summary of odour-evoked $[Ca^{2+}]_i$ responses in a large number of MCs and GCs. Fluorescence traces of individual cells are colour coded and then sorted with respect to their response pattern. Five responses are exemplified in both representations. Odour-elicited decreases in somatic $[Ca^{2+}]_i$ (shown in blue) occur more often in MCs than in GCs.

of APs in different cell types of the OB. In MCs, $[Ca^{2+}]_i$ increments are precisely correlated with spikes down to the single spike level. In contrast, GCs show a lower degree of correlation and a more complex $[Ca^{2+}]_i$ -spiking relationship. Thus, whereas somatic $[Ca^{2+}]_i$ recordings can serve as a powerful tool to detect spikes in MCs, they do not reliably indicate the occurrence of APs in other cell types such as GCs. Given the enormous variety of cell types in the central nervous system, similar variations in the $[Ca^{2+}]_i$ -spiking relationship presumably occur in many other brain regions.

Relationship between somatic $[Ca^{2+}]_i$ and APs

Calcium imaging at high temporal resolution demonstrates that rising phases of the $[Ca^{2+}]_i$ signal contain step-like $[Ca^{2+}]_i$ increments (Fig. 6C), which correlate precisely with the occurrence of individual APs

in MCs (see Result and Fig. 6). The precise correlation of individual APs and small $[Ca^{2+}]_i$ increments strongly suggests a coupling between these two activities via voltage-activated calcium channels (Markram *et al.* 1995). In contrast to MCs, cells in the granule cell layer show a much lower correlation between somatic $[Ca^{2+}]_i$ increases and the occurrence of APs. There was either no correlation between the Δr and the numbers of APs or the latency and duration of odour-evoked spike trains did not correspond to the $[Ca^{2+}]_i$ increases (Fig. 7; for a comparison with the rat OB see Kapoor & Urban, 2007).

Several differences between MCs and GCs may underlie such distinct $[Ca^{2+}]_i$ -APs relationships. First, cell bodies of GCs show immunoreactivity to T-type low-threshold calcium channels (mammalian OBs; Yunker *et al.* 2003). These channels can mediate Ca^{2+} influx at subthreshold depolarizations (Egger *et al.* 2005). We have indeed observed prominent Ca^{2+} increases in response to

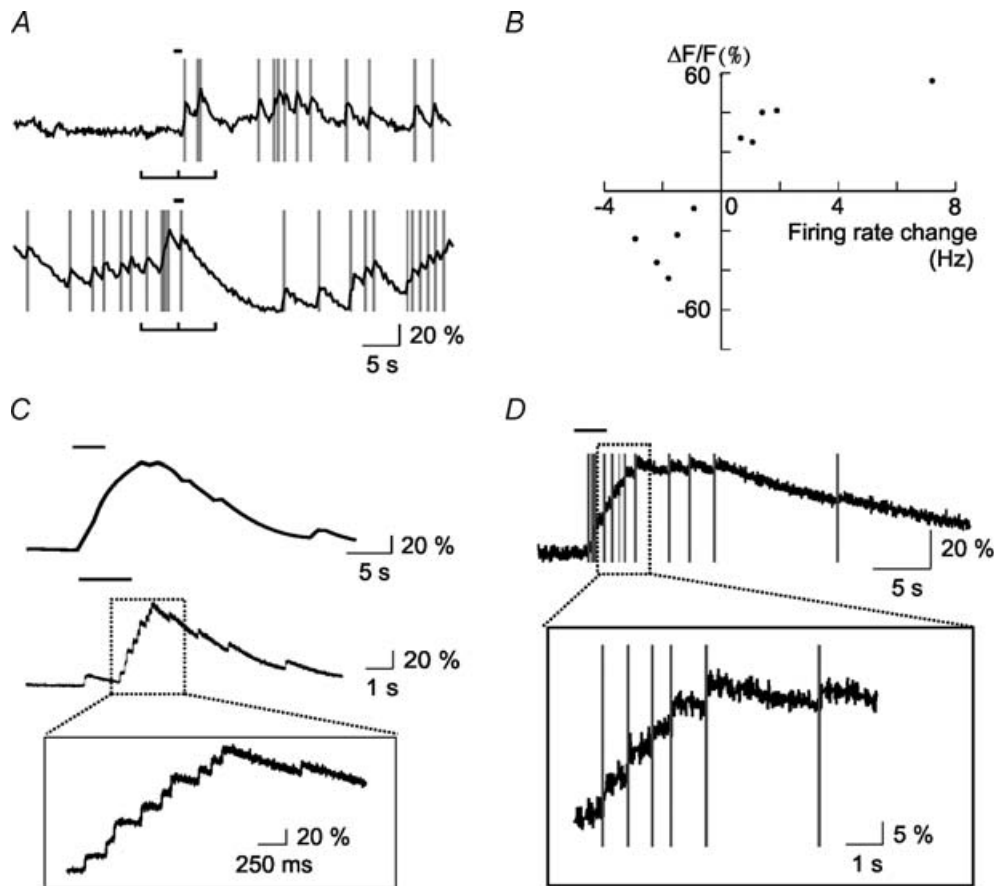


Figure 6. Odour-evoked $[Ca^{2+}]_i$ responses and spikes in MCs

A, odour-elicited spikes coincide with rising phases of the $[Ca^{2+}]_i$ responses (upper trace). Odour-induced suppression of spiking correlated with decrease in somatic $[Ca^{2+}]_i$ (lower trace). B, summary of odour-evoked firing rate and fluorescence changes in all MCs sampled ($n = 10$). Changes in firing rates and $\Delta F/F$ were measured in a 5 s time window immediately before and after stimulation (marked in Fig. 6A). C, calcium imaging at different time resolutions using the line scanning mode of a confocal microscope. Increased resolution shows stepwise $[Ca^{2+}]_i$ increments. D, an MC showing a precise correlation between individual spikes and single $[Ca^{2+}]_i$ steps. Odorant stimulations are indicated as horizontal bars above traces.

subthreshold depolarization (Fig. 9A) and long lasting depolarizations with superimposed fast spikes during odour stimulation in GCs (Fig. 9C). Thus, the activation of T-type calcium channels by subthreshold depolarizations is likely to contribute to the observed somatic $[Ca^{2+}]_i$

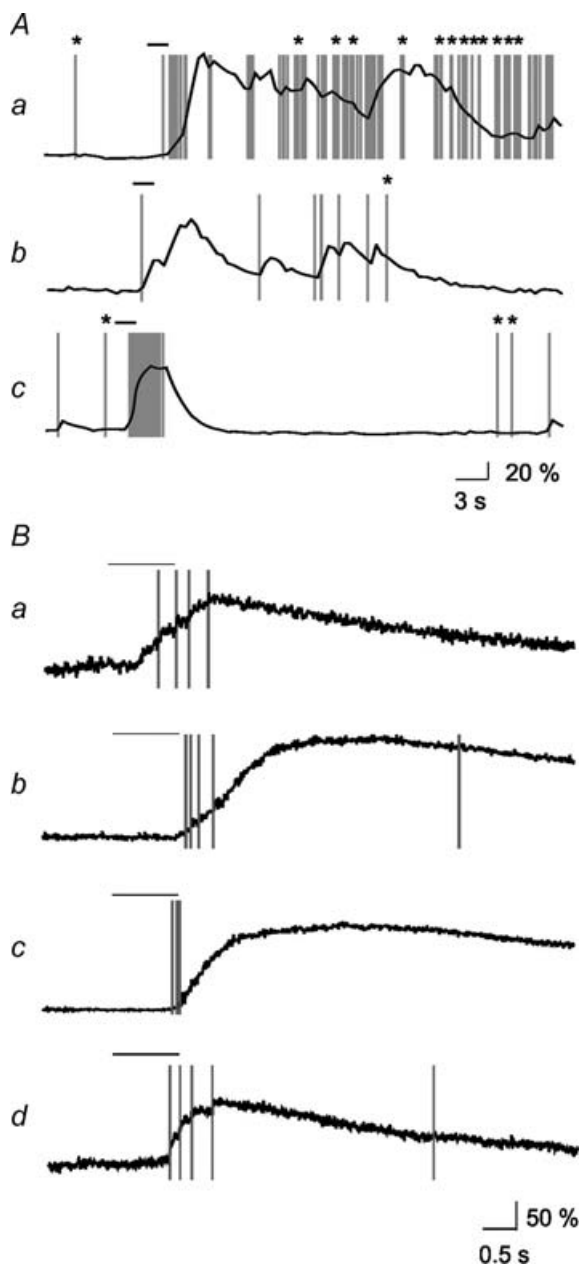


Figure 7. Odour-evoked $[Ca^{2+}]_i$ responses and spikes in GCs
 A, relationships between odour-induced APs and increases in $[Ca^{2+}]_i$. Asterisks indicate spikes without effects upon the $[Ca^{2+}]_i$ trace. Odorant stimulus is indicated by a bar over the trace. B, fast calcium imaging in four GCs with APs superimposed. Cells in a, b, and c lack correlation between odour-evoked spiking and $[Ca^{2+}]_i$ dynamics. A different relationship is observed in the GC in d that shows a strict correlation upon odorant stimulation but no $[Ca^{2+}]_i$ changes upon a latter AP. Odorant stimulus is indicated by a bar over the trace.

fluctuation in the absence of APs (Fig. 7). On the other hand, T-type calcium channels are also known to be fast inactivating in a voltage range similar to that required for its activation (Hille, 2001). In a recent study done in rat GCs, the AP-induced $[Ca^{2+}]_i$ transients in GCs are shown to be attenuated by more than 90% when the membrane holding potential is shifted from -80 mV to -50 mV, presumably due to the inactivation of T-type calcium channels (Egger *et al.* 2003). This goes in line with our observation that GC APs often fail to induce observable $[Ca^{2+}]_i$ transients in the soma, in particular after odorant stimulation (Figs 4, 7Aa, 7Bb and 7Bd). Odorant stimulation could drive the GC membrane potential to a more depolarized range (Fig. 9), which might inactivate T-type calcium channels and consequently attenuates AP-evoked $[Ca^{2+}]_i$ transients to a virtually undetectable level.

Second, focal application of NMDA to cell somata elicits prominent $[Ca^{2+}]_i$ increases in GCs but not in MCs (Fig. 8) suggesting the activation of NMDA channels as an additional mechanism underlying the complex

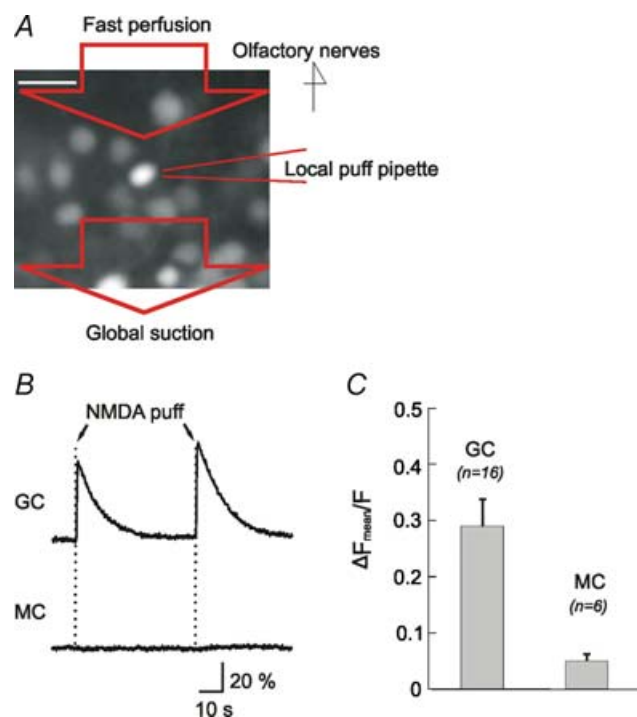


Figure 8. NMDA puff elicits $[Ca^{2+}]_i$ increases in GCs but not in MCs

A, focal puff of NMDA is applied onto a cell body of an OB neuron. A fast perfusion system is placed in the vicinity of the puffer pipette for creating an anterior-to-posterior flow of bath solution. B, upon an NMDA puff onto the cell soma, an GC shows a increase in $[Ca^{2+}]_i$ and then a decay to the base level. In contrast, an MC shows no $[Ca^{2+}]_i$ responses to NMDA. C, summary of the $[Ca^{2+}]_i$ responses in all MCs and GCs tested. Despite a response heterogeneity within the GC group, the mean fluorescence change ($\Delta F_{mean}/F$) in GCs is significantly larger than that in MCs ($P < 0.01$).

$[Ca^{2+}]_i$ -spiking relationship in GCs. NMDA channels on GC somata may be activated by the glutamate spilling over from the excited collateral branches of MC axons during stimulation (Shepherd & Greer, 1998). Ca^{2+} influx through NMDA channels may directly contribute to the AP-independent $[Ca^{2+}]_i$ elevation or activate Ca^{2+} -dependent K^+ conductance (Isaacson & Murphy, 2001), leading to a hyperpolarization and the suppression of AP generation.

Heterogeneity among cells in the GC layer

The observation of a low $[Ca^{2+}]_i$ -spiking correlation in the majority but not all cells in the granule cell layer suggests a functional heterogeneity of this cell population. Such heterogeneity was also found in the NMDA puff experiments where 75% of all tested GCs showed NMDA-induced Ca^{2+} influx whereas the remaining 25% did not. Previous studies in rats have identified different types of interneurons in the GC layer (Lopez-Mascaraque *et al.* 1986; Alonso *et al.* 2001; Pressler & Strowbridge, 2006) and described the migration of GCs (Carleton *et al.* 2003; for a review see Alvarez-Buylla & Garcia-Verdugo, 2002) and newborn MCs through the GC layer (Hinds, 1968*a,b*). In *Xenopus*, the number of OB neurons continues to

increase from larval stage 43 till adulthood (Byrd & Burd, 1991), which implies the recruitment and migration of MCs. Thus, neurons in the GC layer are expected to be heterogeneous and have different $[Ca^{2+}]_i$ handling mechanisms that underlie the different $[Ca^{2+}]_i$ -spiking relationships in these neurons.

Imaging individual APs in neuron ensembles showing correlation between APs and $[Ca^{2+}]_i$

Precise correlation between distinct $[Ca^{2+}]_i$ increments and individual APs suggest an intriguing possibility for using the somatic $[Ca^{2+}]_i$ signal to reconstruct the precise timing of APs in many neurons recorded simultaneously. This is certainly interesting in the olfactory system where it has been suggested that, in addition to the firing rate, the precise timing of individual APs is important and could contain relevant odorant information (Wehr & Laurent, 1996; Laurent, 1999).

More generally, calcium imaging at high acquisition rates (Bullen & Saggau, 1999; Takashima *et al.* 1999; Iyer *et al.* 2006) will serve as a powerful tool to investigate spatial patterns of spiking activity as well as temporal coding in many neuronal networks, provided there is a tight $[Ca^{2+}]_i(t)$ -spiking coupling.

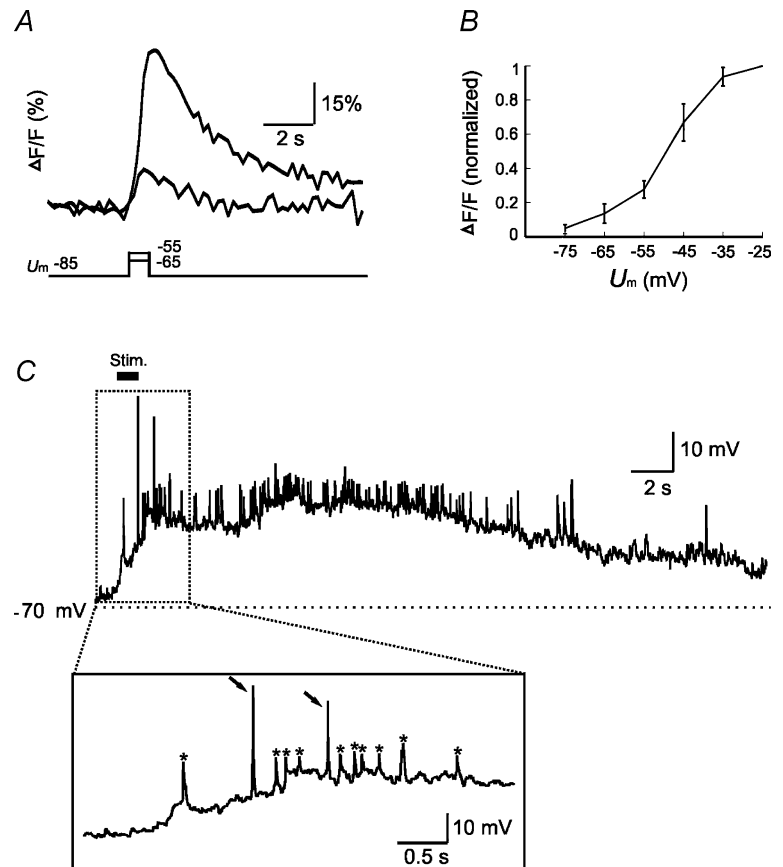


Figure 9. $[Ca^{2+}]_i$ transients evoked by subthreshold depolarization and odour-induced subthreshold dynamics in GC membrane potential. *A*, $[Ca^{2+}]_i$ transients elicited by subthreshold voltage pulses from -85 to -65 and -55 mV in a GC soma. *B*, amplitudes of the transients evoked by various pulses, presented as the percentage of the maximum response amplitude ($\Delta F/F$; normalized) in each cell. *C*, whole-cell voltage-clamp recording reveals complex membrane potential dynamics upon odorant stimulation, including suprathreshold APs (arrows, inset), subthreshold fast depolarizing events (asterisks) and slow depolarizing shift of resting membrane potential ($n = 3$).

References

- Alonso JR, Brinon JG, Crespo C, Bravo IG, Arevalo R & Aijon J (2001). Chemical organization of the macaque monkey olfactory bulb. II. Calretinin, calbindin D-28k, parvalbumin, and neurocalcin immunoreactivity. *J Comp Neurol* **432**, 389–407.
- Alvarez-Buylla A & Garcia-Verdugo JM (2002). Neurogenesis in adult subventricular zone. *J Neurosci* **22**, 629–634.
- Bullen A & Saggau P (1999). High-speed, random-access fluorescence microscopy. II. Fast quantitative measurements with voltage-sensitive dyes. *Biophys J* **76**, 2272–2287.
- Byrd CA & Burd GD (1991). Development of the olfactory bulb in the clawed frogs, *Xenopus laevis*: a morphological and quantitative analysis. *J Comp Neurol* **314**, 79–90.
- Cang J & Isaacson JS (2003). In vivo whole-cell recording of odor-evoked synaptic transmission in the rat olfactory bulb. *J Neurosci* **23**, 4108–4116.
- Carleton A, Petreanu LT, Lansford R, Alvarez-Buylla A & Lledo PM (2003). Becoming a new neuron in the adult olfactory bulb. *Nat Neurosci* **6**, 507–518.
- Chen TW, Lin BJ, Brunner E & Schild D (2006). In situ background estimation in quantitative fluorescence imaging. *Biophys J* **90**, 2534–2547.
- Czesnik D, Nezhlin L, Rabba J, Muller B & Schild D (2001). Noradrenergic modulation of calcium currents and synaptic transmission in the olfactory bulb of *Xenopus laevis* tadpoles. *Eur J Neurosci* **13**, 1093–1100.
- Czesnik D, Rossler W, Kirchner F, Gennerich A & Schild D (2003). Neuronal representation of odourants in the olfactory bulb of *Xenopus laevis* tadpoles. *Eur J Neurosci* **17**, 113–118.
- Egger V, Svoboda K & Mainen ZF (2003). Mechanisms of lateral inhibition in the olfactory bulb: efficiency and modulation of spike-evoked Ca^{2+} influx into granule cells. *J Neurosci* **23**, 7551–7558.
- Egger V, Svoboda K & Mainen ZF (2005). Dendrodendritic synaptic signals in olfactory bulb granule cells: local spine boost and global low-threshold spike. *J Neurosci* **25**, 3521–3530.
- Hille B (2001). *Ion Channels of Excitable Membranes*, 3rd edn, pp. 95–310. Sinauer, Sunderland, MA, USA.
- Hinds JW (1968a). Autoradiographic study of histogenesis in mouse olfactory bulb. I. Time of origin of neurons and neuroglia. *J Comp Neurol* **134**, 287–304.
- Hinds JW (1968b). Autoradiographic study of histogenesis in mouse olfactory bulb. II. Cell proliferation and migration. *J Comp Neurol* **134**, 305–322.
- Isaacson JS & Murphy GJ (2001). Glutamate-mediated extrasynaptic inhibition: direct coupling of NMDA receptors to Ca^{2+} -activated K^{+} channels. *Neuron* **31**, 1027–1034.
- Iyer V, Hoogland TM & Saggau P (2006). Fast functional imaging of single neurons using random-access multiphoton (RAMP) microscopy. *J Neurophysiol* **95**, 535–545.
- Kapoor V & Urban NN (2007). Glomerulus-specific, long-latency activity in the olfactory bulb granule cell network. *J Neurosci* **26**, 11709–11719.
- Kovalchuk Y, Eilers J, Lisman J & Konnerth A (2000). NMDA receptor-mediated subthreshold Ca^{2+} signals in spines of hippocampal neurons. *J Neurosci* **20**, 1791–1799.
- Kuba K, Nohmi M & Hua SY (1992). Intracellular Ca^{2+} dynamics in response to Ca^{2+} influx and Ca^{2+} release in autonomic neurons. *Can J Physiol Pharmacol* **70** (Suppl.), S64–S72.
- Laurent G (1999). A systems perspective on early olfactory coding. *Science* **286**, 723–728.
- Lopez-Mascaraque L, De Carlos JA & Valverde F (1986). Structure of the olfactory bulb of the hedgehog (*Erinaceus europaeus*): description of cell types in the granular layer. *J Comp Neurol* **253**, 135–152.
- Markram H, Helm PJ & Sakmann B (1995). Dendritic calcium transients evoked by single back-propagating action potentials in rat neocortical pyramidal neurons. *J Physiol* **485**, 1–20.
- Nezhlin LP & Schild D (2000). Structure of the olfactory bulb in tadpoles of *Xenopus laevis*. *Cell Tissue Res* **302**, 21–29.
- Nieuwkoop PD & Faber J (1956). *Normal Tables of Xenopus laevis (Daudin)*. North-Holland, Amsterdam.
- Ohki K, Chung S, Ch'ng YH, Kara P & Reid RC (2005). Functional imaging with cellular resolution reveals precise micro-architecture in visual cortex. *Nature* **433**, 597–603.
- Perez-Reyes E (2003). Molecular physiology of low-voltage-activated T-type calcium channels. *Physiol Rev* **83**, 117–161.
- Pinato G & Midtgaard J (2003). Regulation of granule cell excitability by a low-threshold calcium spike in turtle olfactory bulb. *J Neurophysiol* **90**, 3341–3351.
- Pinato G & Midtgaard J (2005). Dendritic sodium spikelets and low-threshold calcium spikes in turtle olfactory bulb granule cells. *J Neurophysiol* **93**, 1285–1294.
- Pressler RT & Strowbridge BW (2006). Blanes cells mediate persistent feedforward inhibition onto granule cells in the olfactory bulb. *Neuron* **49**, 889–904.
- Robert C, Tseeb V, Kordon C & Hammond C (1999). Patch-clamp-induced perturbations of $[\text{Ca}^{2+}]_i$ activity in somatotropes. *Neuroendocrinology* **70**, 343–352.
- Sah P (1996). Ca^{2+} -activated K^{+} currents in neurons: types, physiological roles and modulation. *Trends Neurosci* **19**, 150–154.
- Schild D (1985). A computer-controlled device for the application of odors to aquatic animals. *J Electrophysiol Techniques* **12**, 71–79.
- Shepherd GM & Greer CA (1998). The olfactory bulb. In *The Synaptic Organization of the Brain*, 3rd edn, ed. Shepherd GM, pp. 159–203. Oxford University Press, New York.
- Sullivan MR, Nimmerjahn A, Sarkisov DV, Helmchen F & Wang SS (2005). In vivo calcium imaging of circuit activity in cerebellar cortex. *J Neurophysiol* **94**, 1636–1644.
- Takashima I, Ichikawa M & Iijima T (1999). High-speed CCD imaging system for monitoring neural activity in vivo and in vitro, using a voltage-sensitive dye. *J Neurosci Meth* **91**, 147–159.
- Wehr M & Laurent G (1996). Odour encoding by temporal sequences of firing in oscillating neural assemblies. *Nature* **384**, 162–166.
- Yunker AM, Sharp AH, Sundarraj S, Ranganathan V, Copeland TD & McEnery MW (2003). Immunological characterization of T-type voltage-dependent calcium channel $\text{CaV}3.1$ (alpha 1G) and $\text{CaV}3.3$ (alpha 1I) isoforms reveal differences in their localization, expression, and neural development. *Neuroscience* **117**, 321–335.

- Zelles T, Boyd JD, Hardy AB & Delaney KR (2006). Branch-specific Ca^{2+} influx from Na^+ -dependent dendritic spikes in olfactory granule cells. *J Neurosci* **26**, 30–40.
- Zippel HP & Breipohl W (1975). Functions of the olfactory system in the goldfish (*Carassius auratus*). In *Olfaction and Taste*, ed. Denton DA & Coghlan JP, pp. 163–167. Academic Press, New York.
- Zufall F, Leinders-Zufall T & Greer CA (2000). Amplification of odor-induced Ca^{2+} transients by store-operated Ca^{2+} release and its role in olfactory signal transduction. *J Neurophysiol* **83**, 501–512.

Acknowledgements

We thank W. Stühmer and E. Fuchs for discussions and H. Schulters for reading the manuscript. This work was supported by grants of the DFG Research Center Molecular Physiology of

the Brain and the Bernstein Center for Computational Neuroscience to D.S..

Supplemental material

Online supplemental material for this paper can be accessed at: <http://jp.physoc.org/cgi/content/full/jphysiol.2006.125963/DC1> and <http://www.blackwell-synergy.com/doi/suppl/10.1113/jphysiol.2006.125963>

Movie 1. Focal puff of solution on a cell soma

A movie showing delivery of a brief puff of fluorescent solution. A short pressure pulse (3.4 kPa, 1 s) is applied to a puffer pipette (on the left) to eject the solution. The tip of the pipette is placed against a soma whose contour is drawn on the right side of the pipette. The movie is recorded at 2 frames s^{-1} . Scale bar: $8 \mu\text{m}$.

**Cell type-specific relationships between spiking and [Ca²⁺]_i in neurons of the
Xenopus tadpole olfactory bulb**

Bei-Jung Lin, Tsai-Wen Chen and Detlev Schild

J. Physiol. 2007;582;163-175; originally published online Apr 26, 2007;

DOI: 10.1113/jphysiol.2006.125963

This information is current as of August 8, 2007

Updated Information & Services	including high-resolution figures, can be found at: http://jp.physoc.org/cgi/content/full/582/1/163
Supplementary Material	Supplementary material can be found at: http://jp.physoc.org/cgi/content/full/jphysiol.2006.125963/DC1
Subspecialty Collections	This article, along with others on similar topics, appears in the following collection(s): Neuroscience http://jp.physoc.org/cgi/collection/neuroscience
Permissions & Licensing	Information about reproducing this article in parts (figures, tables) or in its entirety can be found online at: http://jp.physoc.org/misc/Permissions.shtml
Reprints	Information about ordering reprints can be found online: http://jp.physoc.org/misc/reprints.shtml